

Odd entanglement entropy in boundary conformal field theories and holographic moving mirrors

Anjali Kumari*, Vinayak Raj† and Gautam Sengupta‡

Department of Physics,
Indian Institute of Technology,
Kanpur 208 016, India

Abstract

In this article, we investigate the entanglement structure of bipartite mixed states in (1+1)-dimensional boundary conformal field theories (BCFT₂s) through the odd entanglement entropy (OEE) by employing an appropriate replica technique. In this regard we compare our results with the bulk entanglement wedge cross section (EWCS) for AdS₃ geometries with an end-of-the-world brane. We observe consistent extension of the holographic duality between the difference of the OEE and the entanglement entropy (EE) with the bulk EWCS, in the framework of AdS₃/BCFT₂ holography. Furthermore, we also extend our computations to the holographic moving mirror models where the Hawking radiation from eternal and evaporating black holes may be simulated depending on certain mirror profiles, and find consistent extension of the aforementioned holographic duality.

arXiv:2310.11242v1 [hep-th] 17 Oct 2023

*E-mail: anjali07kumariph@gmail.com

†E-mail: vraj@iitk.ac.in

‡E-mail: sengupta@iitk.ac.in

Contents

1	Introduction	3
2	Review of earlier literature	4
2.1	Odd entanglement entropy	4
2.2	Boundary conformal field theory	4
2.3	Holographic moving mirror	5
3	OEE in BCFT₂	6
3.1	OEE for two disjoint subsystems	7
3.1.1	Phase-I	7
3.1.2	Phase-II	9
3.1.3	Phase-III	10
3.2	OEE for two adjacent subsystems	11
3.2.1	Phase-I	12
3.2.2	Phase-II	13
4	Summary and conclusions	15

1 Introduction

The characterization of quantum entanglement in quantum many body systems has become pivotal in investigating a wide range of phenomena, spanning from condensed matter physics to quantum gravity. In quantum information theory, the entanglement entropy (EE) has emerged as a useful measure to quantify the entanglement in bipartite states. The EE is defined as the von-Neumann entropy for the reduced density matrix corresponding to the bipartite quantum state. The computation of the EE is straightforward for finite quantum systems. However, for quantum many body systems, it becomes intractable due to infinite number of eigenvalues for the reduced density matrix in question. An appropriate replica technique to obtain the EE for such field theories was forwarded in [1, 2] where the authors constructed a replicated manifold to obtain the EE in certain replica limit.

The EE properly characterizes the entanglement for bipartite pure states only as it receives irrelevant classical and quantum contributions for mixed states. Thus a different correlation or entanglement measure is required to investigate the entanglement structure of bipartite mixed states. Several such computable quantities has been introduced in the literature, like the entanglement negativity [3, 4], the entanglement of purification [5, 6], the reflected entropy [7], the balanced partial entanglement [8], etc. Another computable measure introduced in [9] is termed as the *odd entanglement entropy* (OEE) which may be interpreted as the von-Neumann entropy of a partially transposed density matrix. A replica technique was provided to obtain the OEE for (1+1)-dimensional field theories with conformal symmetry (CFT₂). In the context of AdS/CFT correspondence [10, 11], the authors in [9] also proposed that the difference of the OEE and the EE in CFT_{dS} may be described holographically through the bulk entanglement wedge cross section (EWCS) in AdS_{d+1} geometries. The OEE has further been explored in various contexts in [12–17].

On a separate note, the study of CFTs on manifolds with boundaries, termed as boundary conformal field theories (BCFTs) [18], have gained importance in recent past due to its application in vast range of topics ranging from the physics of open strings and D-branes to boundary critical behaviour of condensed matter systems. In (1+1)-dimensions, it may be obtained by introducing a conformally invariant boundary on the complex plane, thus preserving one copy of the Virasoro symmetry algebra [18, 19]. The holographic duality for such theories is dubbed as the AdS/BCFT correspondence [20, 21] where the bulk dual is described by an AdS space truncated by an end-of-the-world (EOW) brane with Neumann boundary condition.

Recently in [22, 23], the model of holographic moving mirrors in a BCFT₂ was employed to investigate the black hole information loss problem¹. The authors considered certain profiles for the trajectory of a moving mirror in a complex plane which simulated the Hawking radiation from a black hole. The mirror acts as the boundary of the manifold and produces a radiation flux which may mimic the Hawking radiation from an eternal black hole, an evaporating black hole, or two evaporating black holes depending upon the mirror profile. In this setup, they reproduced the unitary Page curve for the entanglement entropy of a subsystem in the radiation flux of the moving mirrors. It is possible to map this moving mirror setup to a BCFT₂ on a half plane through a conformal transformation which simplifies the computations. Further interesting studies in this direction have been explored in [29–36]

Noting the above developments, the study of the mixed state entanglement in BCFT₂s and its extension to the holographic moving mirror model becomes a natural point of enquiry. This was investigated in [33] through the reflected entropy and the entanglement negativity. But the investigation of the OEE in this setup and the validity of its holographic duality remains an open question and is the main focus of this article. In this context, we obtain the OEE for bipartite adjacent and disjoint subsystems in BCFT₂s through an appropriate replica technique

¹Note that the moving mirror model has earlier been utilized to investigate the information loss problem in [24–28]

and compare the difference between the OEE and the EE with the corresponding EWCS obtained earlier in [33, 37, 38]. We further extend our results to the holographic moving mirror setup by utilizing certain conformal transformations and again compare our results with earlier literature. Moreover, we plot the variation of the difference between the OEE and the EE with time to observe the transition between various phases, for mirror profiles simulating an evaporating and an eternal black hole.

The rest of the article is arranged as follows. In section 2, we provide a brief review of the several individual elements utilized in this study. Further in section 3, we provide an appropriate replica technique and obtain the OEE for two adjacent and two disjoint subsystems in BCFT_{2S} in various phases. We also extend our computations to the moving mirror setup for all the cases discussed. Finally, in section 4, we summarize our results and draw conclusions.

2 Review of earlier literature

2.1 Odd entanglement entropy

We begin with a brief review of the bipartite correlation measure termed as the odd entanglement entropy (OEE), introduced in [9]. It could be understood as the von Neumann entropy of the partially transposed reduced density matrix of the given bipartite state. For a more precise definition, begin by considering a tripartite pure state composed of the subsystems A_1 , A_2 , and B . Subsequently, a bipartite mixed state is prepared by tracing out the degrees of freedom of the subsystem B to obtain the reduced density matrix $\rho_{A_1 A_2}$ defined on the Hilbert space $\mathcal{H} = \mathcal{H}_{A_1} \otimes \mathcal{H}_{A_2}$. The partial transposition of the reduced density matrix $\rho_{A_1 A_2}$ with respect to the subsystem A_2 is then defined as

$$\left\langle e_i^{(1)} e_j^{(2)} \left| \rho_{A_1 A_2}^{T_{A_2}} \right| e_k^{(1)} e_l^{(2)} \right\rangle = \left\langle e_i^{(1)} e_l^{(2)} \left| \rho_{A_1 A_2} \right| e_k^{(1)} e_j^{(2)} \right\rangle. \quad (2.1)$$

where $|e_i^{(1)}\rangle$ and $|e_j^{(2)}\rangle$ are the orthogonal bases for the Hilbert spaces \mathcal{H}_{A_1} and \mathcal{H}_{A_2} respectively. Further, the Rényi generalization of the OEE for the partially transposed density matrix is defined as follows

$$S_o^{(n_o)}(A_1 : A_2) = \frac{1}{1 - n_o} \log \left[\text{Tr} \left(\rho_{A_1 A_2}^{T_{A_2}} \right)^{n_o} \right], \quad (2.2)$$

where n_o is an odd integer². The odd entanglement entropy S_o for the given mixed state $\rho_{A_1 A_2}$ may finally be obtained through the analytic continuation of the odd integer $n_o \rightarrow 1$ in the above expression as follows

$$S_o(A_1 : A_2) = \lim_{n_o \rightarrow 1} \left[S_o^{(n_o)}(A_1 : A_2) \right]. \quad (2.3)$$

Moreover, in the context of the AdS/CFT correspondence, the difference between the OEE and the EE has been conjectured to be described holographically in terms of the bulk EWCS corresponding to the bipartite state under consideration, as follows [9]

$$S_o(A_1 : A_2) - S(A_1 \cup A_2) = E_W(A_1 : A_2) \quad (2.4)$$

where $S(A_1 \cup A_2)$ denotes the EE and $E_W(A_1 : A_2)$ denotes the EWCS for the subsystem $A_1 \cup A_2$.

2.2 Boundary conformal field theory

Boundary conformal field theory (BCFT) is a CFT defined on manifolds with a boundary. This may be defined in $(1+1)$ -dimensions by considering a CFT₂ on the half-plane $x \geq 0$. This

²The trace in eq. (2.2) may be obtained in a CFT₂ through a correlation function of twist fields Φ_n as will be discussed in section 3 in the context of boundary conformal field theories.

BCFT₂ defined on the right half plane (RHP) preserves one copy of the Virasoro symmetry algebra of a usual CFT and it corresponds to a set of generators given by [18–21]

$$\tilde{L}_n = L_n + \bar{L}_n, \quad (2.5)$$

where L_n and \bar{L}_n are the generators of the two copies of Virasoro algebra of the usual CFT₂.

Any n -point correlation function in such BCFT₂s may be described by a $2n$ -point correlator in the chiral CFT on the whole complex plane through the Cardy's *doubling trick*³ as follows [18]

$$\langle \mathcal{O}_{h_1 \bar{h}_1}(z_1, \bar{z}_1) \cdots \mathcal{O}_{h_n \bar{h}_n}(z_n, \bar{z}_n) \rangle_{\text{BCFT}} \sim \langle \mathcal{O}_{h_1}(z_1) \cdots \mathcal{O}_{h_n}(z_n) \mathcal{O}_{\bar{h}_1}(\bar{z}_1) \cdots \mathcal{O}_{\bar{h}_n}(\bar{z}_n) \rangle_{\text{CFT}}, \quad (2.6)$$

where h_i, \bar{h}_i represent the conformal dimensions of the operator \mathcal{O} at position z_i . This doubling trick leads to a non-vanishing one-point function for a scalar primary operator in the BCFT₂ which is given as

$$\langle \mathcal{O}_{h\bar{h}}(z, \bar{z}) \rangle_{\text{BCFT}} = \frac{A_{\mathcal{O}}}{|z - z^*|^{\Delta}} = \frac{A_{\mathcal{O}}}{|2y|^{\Delta}}, \quad (2.7)$$

where $z = x + iy$, $\Delta = h + \bar{h}$ is the scaling dimension of the operator \mathcal{O} and $A_{\mathcal{O}}$ is the normalization of the two-point function. Correspondingly, a two-point function on the half plane may be expressed in two different channels based on the location of the primary operators, here illustrated through twist-field operators, as follows

$$\langle \Phi_n(z_1, \bar{z}_1) \bar{\Phi}_n(z_2, \bar{z}_2) \rangle_{\text{BCFT}} = \begin{cases} \frac{g_b^{2(1-n)} \epsilon^{2\Delta_n}}{(4y_1 y_2)^{\Delta_n}} & \eta \rightarrow 0, \\ \frac{\epsilon^{2\Delta_n}}{|z_1 - z_2|^{2\Delta_n}} & \eta \rightarrow 1, \end{cases} \quad (2.8)$$

where Δ_n is the scaling dimension of the twist field Φ_n and g_b is the (regulated) partition function for the CFT on a disk with depend on the set boundary condition and is related to the boundary entropy [19]. The cross-ratio η in the previous expression is given by

$$\eta = \frac{(z_1 - \bar{z}_1)(z_2 - \bar{z}_2)}{(z_1 - \bar{z}_2)(z_2 - \bar{z}_1)}. \quad (2.9)$$

2.3 Holographic moving mirror

In this subsection, we briefly review the holographic moving mirror model discussed in [22, 23]. The authors considered certain mirror trajectories described by the profile $x = Z(t)$ which mimic the Hawking radiation from eternal as well as evaporating black holes. The mirror acts as a boundary and the region to its right is described by a BCFT₂. This BCFT is mapped to a right-half-plane (RHP) through the following conformal transformation of the light cone coordinates $u = t - x$ and $v = t + x$,

$$\tilde{u} = p(u), \quad \tilde{v} = v, \quad (2.10)$$

where the function $p(u)$ is chosen such that the mirror becomes static $\tilde{u} - \tilde{v} = 0$, i.e., $v = p(u)$. In the original coordinates, this may be expressed as

$$t + Z(t) = p(t - Z(t)). \quad (2.11)$$

³An alternative way to compute the BCFT correlator termed as the *mirror method*, has been described in [23] where $\langle \sigma\sigma \rangle_{\text{BCFT}} \simeq \sqrt{\langle \sigma\sigma\sigma\sigma \rangle_{\text{CFT}}}$ with the four-point correlator being computed in the usual CFT (with both holomorphic and anti-holomorphic part) and not in the chiral CFT.

The stress tensor in the tilde coordinates may be obtained by noting that the BCFT in the RHP is in the ground state. Thus, for the map in eq. (2.10), the stress tensor is only given by the conformal anomaly as follows

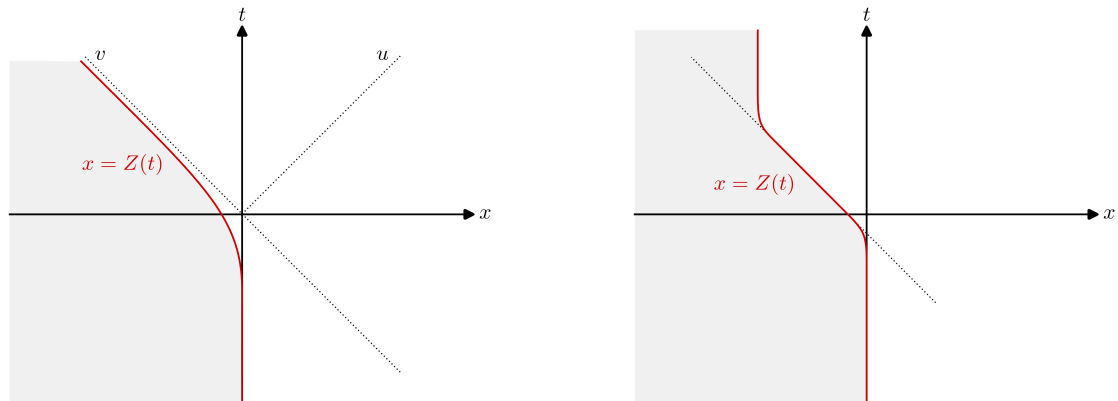
$$T_{uu} = \frac{c}{24} \left(\frac{3}{2} \left(\frac{p''(u)}{p'(u)} \right)^2 - \frac{p'''(u)}{p'(u)} \right), \quad (2.12)$$

where primes represent derivatives with respect to u .

As stated earlier, these holographic moving mirror setups could simulate the Hawking radiation from black holes. In particular, an eternal black hole with inverse temperature β is modelled by considering an escaping mirror for which the profile is given by [22, 23]

$$p(u) = -\beta \log \left(1 + e^{-\frac{u}{\beta}} \right). \quad (2.13)$$

As depicted in fig. 1a, in the early time limit $t \rightarrow 0$, the mirror is static $Z(t) \simeq 0$, whereas at late times $t \rightarrow \infty$, the mirror trajectory becomes almost null $Z(t) \simeq -t - \beta e^{-2\frac{t}{\beta}}$. On the other hand,



(a) Schematics of the escaping mirror configuration modelling an eternal black hole.

(b) Schematics of the kink mirror configuration modelling an evaporating black hole.

Figure 1: Two mirror configurations simulating the Hawking radiation from black holes. The red curves describe the mirror trajectories.

an evaporating single-sided black holes is simulated by a kink mirror setup with the following profile [22, 23]

$$p(u) = -\beta \log \left(1 + e^{-\frac{u}{\beta}} \right) + \beta \log \left(1 + e^{\frac{u-u_0}{\beta}} \right), \quad (2.14)$$

where $u_0 > 0$. In the large temperature limit $\beta \rightarrow 0$, the mirror trajectory is depicted in fig. 1b and may be approximated as

$$Z(t) \simeq \begin{cases} 0 & t < 0, \\ -t & 0 \leq t \leq \frac{u_0}{2}, \\ -\frac{u_0}{2} & t > \frac{u_0}{2}. \end{cases} \quad (2.15)$$

In the next section, we will now develop the replica technique for the OEE in BCFT₂ in order to investigate the nature of bipartite mixed state entanglement through the OEE in moving mirror models.

3 OEE in BCFT₂

We will now establish the replica technique to obtain the OEE for bipartite states in BCFT₂s. To this end, consider the generic configuration of two disjoint subsystems $A_1 \equiv [x_1, x_2]$ and

$A_2 \equiv [x_3, x_4]$ on a half-plane $x \geq 0$. Following [2, 9, 39], the trace $\text{Tr}\left(\rho_{A_1 A_2}^{T_{A_2}}\right)^{n_0}$ of the partially transposed reduced density matrix in the Rényi OEE in eq. (2.2), may be obtained through a correlation function on twist field operators placed at the end points of the subsystems on the half-plane as follows

$$\text{Tr}\left(\rho_{A_1 A_2}^{T_{A_2}}\right)^{n_0} = \langle \mathcal{T}_{n_0}(x_1) \bar{\mathcal{T}}_{n_0}(x_2) \bar{\mathcal{T}}_{n_0}(x_3) \mathcal{T}_{n_0}(x_4) \rangle_{\text{BCFT}}. \quad (3.1)$$

Here \mathcal{T}_{n_0} and $\bar{\mathcal{T}}_{n_0}$ are the twist and anti-twist field operators in BCFT_2 respectively, with the scaling dimension $\Delta_{\mathcal{T}_{n_0}}$ as

$$\Delta_{\mathcal{T}_{n_0}} = h_{\mathcal{T}_{n_0}} + \bar{h}_{\bar{\mathcal{T}}_{n_0}} = \frac{c}{12} \left(n_0 - \frac{1}{n_0} \right). \quad (3.2)$$

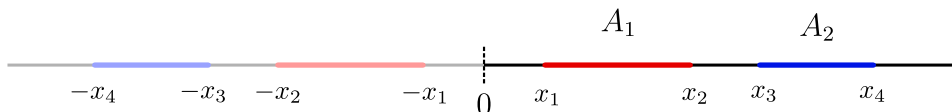


Figure 2: Two disjoint subsystems A_1 and A_2 in BCFT_2 with boundary at $x = 0$. The darker region to the right ($x > 0$) represent the BCFT_2 and the lighter region to the left ($x < 0$) represent the copy obtained after utilizing the doubling trick.

In the following subsections, we will now compute the OEE for two disjoint and two adjacent subsystems in BCFT_2 s in different phases depending upon the location and size of the subsystems under consideration. We will further use the transformations in eq. (2.10) to map the results to the moving mirror setup.

3.1 OEE for two disjoint subsystems

We will now compute the OEE for the mixed state configuration of two disjoint subsystems $A_1 \equiv [x_1, x_2]$ and $A_2 \equiv [x_3, x_4]$ in a BCFT_2 as shown in fig. 2. In this scenario, the four-point function on the half-plane in eq. (3.1) may be described by an eight-point correlator in the chiral CFT via the doubling trick, as follows

$$\begin{aligned} & \langle \mathcal{T}_{n_0}(x_1) \bar{\mathcal{T}}_{n_0}(x_2) \bar{\mathcal{T}}_{n_0}(x_3) \mathcal{T}_{n_0}(x_4) \rangle_{\text{BCFT}} \\ & \sim \langle \mathcal{T}_{n_0}(x_1) \bar{\mathcal{T}}_{n_0}(x_2) \bar{\mathcal{T}}_{n_0}(x_3) \mathcal{T}_{n_0}(x_4) \bar{\mathcal{T}}_{n_0}(-x_1) \mathcal{T}_{n_0}(-x_2) \bar{\mathcal{T}}_{n_0}(-x_3) \mathcal{T}_{n_0}(-x_4) \rangle_{\text{CFT}}. \end{aligned} \quad (3.3)$$

In the large- c limit, the above eight-point twist correlator factorizes based upon the sizes and the locations of the subsystems. We will now discuss several of these phases in the following.

3.1.1 Phase-I

We begin by considering the two subsystems to be close to the boundary such that the separation between them is also small. In this scenario, the four-point BCFT correlator in eq. (3.3) factorizes in the large- c limit in the following way

$$\langle \mathcal{T}_{n_0}(x_1) \bar{\mathcal{T}}_{n_0}(x_2) \bar{\mathcal{T}}_{n_0}(x_3) \mathcal{T}_{n_0}(x_4) \rangle_{\text{BCFT}} \sim \langle \mathcal{T}_{n_0}(x_1) \rangle_{\text{BCFT}} \langle \bar{\mathcal{T}}_{n_0}(x_2) \bar{\mathcal{T}}_{n_0}(x_3) \rangle_{\text{BCFT}} \langle \mathcal{T}_{n_0}(x_4) \rangle_{\text{BCFT}}. \quad (3.4)$$

Using the doubling trick, the one-point functions in the above expression may be computed easily. However, obtaining a general form for the two-point function which corresponds to a four-point twist correlator in the chiral CFT_2 is hard to compute. This computation is simplified in the large- c limit for which the four-point correlator may be expanded in terms of the conformal blocks as follows

$$\frac{\langle \mathcal{T}_{n_0}(-x_2) \bar{\mathcal{T}}_{n_0}(x_2) \bar{\mathcal{T}}_{n_0}(x_3) \mathcal{T}_{n_0}(-x_3) \rangle_{\text{CFT}}}{(x_2 - x_3)^{-\frac{c}{6} \frac{n^2 - 1}{n}}} = \sum_p b_p \mathcal{F}(c, h_{\mathcal{T}_{n_0}}, h_p, 1 - x) \bar{\mathcal{F}}(c, \bar{h}_{\bar{\mathcal{T}}_{n_0}}, \bar{h}_p, 1 - \bar{x}) \quad (3.5)$$

where $x = \frac{(2x_2)(2x_3)}{(x_2+x_3)^2}$ is the cross-ratio, b_p is the OPE coefficient, and \mathcal{F} and $\bar{\mathcal{F}}$ are the Virasoro conformal blocks corresponding to the exchange of the primary operator with conformal dimension h_p . For the given configuration, the dominant contribution comes from the composite twist operator $\bar{\mathcal{T}}_{n_0}^2$ with the conformal weight $h_{\bar{\mathcal{T}}_{n_0}^2} = h_{\mathcal{T}_{n_0}} = \Delta_{\mathcal{T}_{n_0}}/2$. The conformal block corresponding to this operator may then be obtained through the monodromy technique as follows

$$\log \mathcal{F}(c, h_{\mathcal{T}_{n_0}}, h_{\bar{\mathcal{T}}_{n_0}^2}, 1-x) = -h_{\bar{\mathcal{T}}_{n_0}^2} \log \left[\frac{1+\sqrt{x}}{1-\sqrt{x}} \right]. \quad (3.6)$$

The OEE may now be obtained for this phase by utilizing the above conformal block in eq. (3.4), to be

$$S_o(A_1 : A_2) = \frac{c}{6} \left[\log \left(\frac{2x_1}{\epsilon} \right) + 2 \log \left(\frac{x_2 - x_3}{\epsilon} \right) + \log \left(\frac{2x_4}{\epsilon} \right) \right] + \frac{c}{6} \log \left[\left(\frac{\sqrt{x_2} + \sqrt{x_3}}{\sqrt{x_2} - \sqrt{x_3}} \right) \right] + 3S_{\text{bdy}}. \quad (3.7)$$

where S_{bdy} is the boundary entropy representing the entanglement with the boundary degrees of freedom. The corresponding entanglement entropy for this configuration may be obtained as

$$S(A_1 \cup A_2) = \frac{c}{6} \left[\log \left(\frac{2x_1}{\epsilon} \right) + 2 \log \left(\frac{x_2 - x_3}{\epsilon} \right) + \log \left(\frac{2x_4}{\epsilon} \right) \right] + 2S_{\text{bdy}}. \quad (3.8)$$

The OEE modulo the contribution from the entanglement entropy may then be given by

$$S_o(A_1 : A_2) - S(A_1 \cup A_2) = \frac{c}{6} \log \left[\left(\frac{\sqrt{x_2} + \sqrt{x_3}}{\sqrt{x_2} - \sqrt{x_3}} \right) \right] + S_{\text{bdy}}. \quad (3.9)$$

which matches with the corresponding bulk EWCS computed earlier in [33, 37, 38] and is consistent with the holographic duality in eq. (2.4).

Moving mirror

We will now compute the OEE for subsystems $A_1 \equiv [(t, x_1), (t, x_2)]$ and $A_2 \equiv [(t, x_3), (t, x_4)]$ in the moving mirror setup. To this end, we first generalize the result obtained in eq. (3.7) to complex coordinates where the subsystems are located in the RHP at $\tilde{z}_i = (\tilde{t}_i, \tilde{x}_i)$ as follows

$$S_o(A_1 : A_2) = \frac{c}{6} \left[\log \left(\frac{\tilde{z}_1 - \tilde{z}_1^*}{\epsilon} \right) + \log \left(\frac{\tilde{z}_2 - \tilde{z}_3}{\epsilon} \right) + \log \left(\frac{\tilde{z}_2^* - \tilde{z}_3^*}{\epsilon} \right) + \log \left(\frac{\tilde{z}_4 - \tilde{z}_4^*}{\epsilon} \right) \right] + \frac{c}{12} \log \left[\frac{1+\sqrt{\tilde{\eta}}}{1-\sqrt{\tilde{\eta}}} \right] + 3S_{\text{bdy}}. \quad (3.10)$$

where \tilde{z}_i^* represents the complex conjugate of \tilde{z}_i and the modified cross-ratio $\tilde{\eta}$ is given by

$$\tilde{\eta} = \frac{(\tilde{z}_2^* - \tilde{z}_2)(\tilde{z}_3 - \tilde{z}_3^*)}{(\tilde{z}_2^* - \tilde{z}_3)(\tilde{z}_2 - \tilde{z}_3^*)}. \quad (3.11)$$

Now utilizing the inverse of the static map in eq. (2.10), the OEE in the moving mirror setup may be obtained as

$$S_o(A_1 : A_2) = \frac{c}{6} \left[\log \left(\frac{p(t-x_1) - t - x_1}{\epsilon} \right) + \log \left(\frac{p(t-x_2) - p(t-x_3)}{\epsilon} \right) + \log \left(\frac{x_2 - x_3}{\epsilon} \right) \right] + \log \left(\frac{p(t-x_4) - t - x_4}{\epsilon} \right) + \frac{c}{12} \log \left[\frac{1+\sqrt{\tilde{\eta}}}{1-\sqrt{\tilde{\eta}}} \right] + 3S_{\text{bdy}}, \quad (3.12)$$

where $p(u)$ represents the given mirror profile and the cross-ratio η is given by

$$\eta = \frac{(t + x_2 - p(t - x_2))(p(t - x_3) - t - x_3)}{(t + x_2 - p(t - x_3))(p(t - x_2) - t - x_3)}. \quad (3.13)$$

Subtracting the EE contribution from the OEE, we may obtain the following

$$S_o(A_1 : A_2) - S(A_1 \cup A_2) = \frac{c}{12} \log \left[\frac{1 + \sqrt{\eta}}{1 - \sqrt{\eta}} \right] + S_{\text{bdy}}. \quad (3.14)$$

This matches with the corresponding moving mirror result for the EWCS in [33].

3.1.2 Phase-II

In this phase, we consider that the two subsystems are still close to the boundary but the subsystem A_1 is small such that the eight-point chiral correlator in eq. (3.3) factorizes into a four-point correlator and a pair of two-point correlators as follows,

$$\begin{aligned} & \langle \mathcal{T}_{n_0}(x_1) \bar{\mathcal{T}}_{n_0}(x_2) \bar{\mathcal{T}}_{n_0}(x_3) \mathcal{T}_{n_0}(x_4) \bar{\mathcal{T}}_{n_0}(-x_1) \mathcal{T}_{n_0}(-x_2) \mathcal{T}_{n_0}(-x_3) \bar{\mathcal{T}}_{n_0}(-x_4) \rangle_{\text{CFT}} \\ & \sim \langle \mathcal{T}_{n_0}(x_1) \bar{\mathcal{T}}_{n_0}(x_2) \bar{\mathcal{T}}_{n_0}(x_3) \bar{\mathcal{T}}_{n_0}(-x_1) \rangle_{\text{CFT}} \langle \mathcal{T}_{n_0}(x_4) \bar{\mathcal{T}}_{n_0}(-x_4) \rangle_{\text{CFT}} \langle \mathcal{T}_{n_0}(-x_2) \mathcal{T}_{n_0}(-x_3) \rangle_{\text{CFT}}. \end{aligned} \quad (3.15)$$

Note that similar factorization has also been observed in [33] in the context of reflected entropy. For this case also, the four-point correlator may be obtained in the large- x limit through the monodromy technique described earlier. Again, the dominant contribution arises from the twist operator $\bar{\mathcal{T}}_{n_0}^2$ for which the conformal block is as given in eq. (3.6). However the cross-ratio x for the four-point twist correlator in eq. (3.15) in this case is modified to

$$x = \frac{(x_1 - x_2)(x_3 + x_1)}{(x_1 - x_3)(x_2 + x_1)}. \quad (3.16)$$

The OEE may now be obtained to be

$$\begin{aligned} S_o(A_1 : A_2) &= \frac{c}{6} \left[\log \left(\frac{2x_1}{\epsilon} \right) + 2 \log \left(\frac{x_2 - x_3}{\epsilon} \right) + \log \left(\frac{2x_4}{\epsilon} \right) \right] \\ &+ \frac{c}{6} \log \left[\frac{x_2 x_3 - x_1^2 + \sqrt{(x_1^2 - x_3^2)(x_1^2 - x_2^2)}}{x_1(x_3 - x_2)} \right] + 2S_{\text{bdy}}. \end{aligned} \quad (3.17)$$

The corresponding entanglement entropy for this case remains unchanged and is given by eq. (3.8). The difference between the OEE and the EE may then be obtained as

$$S_o(A_1 : A_2) - S(A_1 \cup A_2) = \frac{c}{6} \log \left[\frac{x_1^2 - x_2 x_3 + \sqrt{(x_1^2 - x_3^2)(x_1^2 - x_2^2)}}{x_1(x_2 - x_3)} \right], \quad (3.18)$$

which matches with the corresponding EWCS obtained in [33, 37, 38] and is consistent with the duality in eq. (2.4) for the AdS₃/BCFT₂ scenarios. This provides a consistency check for our computation.

Moving mirror

Generalizing the OEE obtained in eq. (3.17) for complex coordinates $\tilde{z} = (\tilde{t}, \tilde{x})$ in the RHP, we obtain

$$\begin{aligned} S_o(A_1 : A_2) &= \frac{c}{6} \left[\log \left(\frac{\tilde{z}_1 - \tilde{z}_1^*}{\epsilon} \right) + \log \left(\frac{\tilde{z}_2 - \tilde{z}_3}{\epsilon} \right) + \log \left(\frac{\tilde{z}_2^* - \tilde{z}_3^*}{\epsilon} \right) + \log \left(\frac{\tilde{z}_4 - \tilde{z}_4^*}{\epsilon} \right) \right] \\ &+ \frac{c}{6} \log \left[\frac{1 + \sqrt{\tilde{\eta}}}{1 - \sqrt{\tilde{\eta}}} \right] + 2S_{\text{bdy}}, \end{aligned} \quad (3.19)$$

with the modified cross-ratio $\tilde{\eta}$ being given by

$$\tilde{\eta} = \frac{(\tilde{z}_1 - \tilde{z}_2)(\tilde{z}_3 - \tilde{z}_1^*)}{(\tilde{z}_1 - \tilde{z}_3)(\tilde{z}_2 - \tilde{z}_1^*)}. \quad (3.20)$$

We may now utilize the inverse of the static map in eq. (2.10) to obtain the OEE in the moving mirror setup for subsystems $A_1 \equiv [(t, x_1), (t, x_2)]$ and $A_2 \equiv [(t, x_3), (t, x_4)]$ as follows

$$S_o(A_1 : A_2) = \frac{c}{6} \left[\log \left(\frac{p(t-x_1) - t - x_1}{\epsilon} \right) + \log \left(\frac{p(t-x_2) - p(t-x_3)}{\epsilon} \right) + \log \left(\frac{x_2 - x_3}{\epsilon} \right) \right. \\ \left. + \log \left(\frac{p(t-x_4) - t - x_4}{\epsilon} \right) \right] + \frac{c}{6} \log \left[\frac{1 + \sqrt{\eta}}{1 - \sqrt{\eta}} \right] + 2S_{\text{bdy}}, \quad (3.21)$$

where again $p(u)$ represents the given mirror profile for the moving mirror setup and the cross-ratio η is given as

$$\eta = \frac{(p(t-x_1) - p(t-x_2))(p(t-x_3) - t - x_1)}{(p(t-x_1) - p(t-x_3))(p(t-x_2) - t - x_1)}. \quad (3.22)$$

It is now possible to remove the EE contribution from the OEE to obtain the following expression

$$S_o(A_1 : A_2) - S(A_1 \cup A_2) = \frac{c}{6} \log \left[\frac{1 + \sqrt{\eta}}{1 - \sqrt{\eta}} \right]. \quad (3.23)$$

The above matches with the corresponding EWCS in moving mirror setup in [33].

3.1.3 Phase-III

We now consider the case where the subsystems are close to the boundary but the subsystem A_2 is small. This leads to the following factorization of the eight-point chiral correlator in eq. (3.3),

$$\langle \mathcal{T}_{n_0}(x_1) \bar{\mathcal{T}}_{n_0}(x_2) \bar{\mathcal{T}}_{n_0}(x_3) \mathcal{T}_{n_0}(x_4) \bar{\mathcal{T}}_{n_0}(-x_1) \mathcal{T}_{n_0}(-x_2) \mathcal{T}_{n_0}(-x_3) \bar{\mathcal{T}}_{n_0}(-x_4) \rangle_{\text{CFT}} \\ \sim \langle \bar{\mathcal{T}}_{n_0}(x_3) \mathcal{T}_{n_0}(x_4) \bar{\mathcal{T}}_{n_0}(-x_4) \bar{\mathcal{T}}_{n_0}(x_2) \rangle_{\text{CFT}} \langle \mathcal{T}_{n_0}(x_1) \bar{\mathcal{T}}_{n_0}(-x_1) \rangle_{\text{CFT}} \langle \mathcal{T}_{n_0}(-x_2) \mathcal{T}_{n_0}(-x_3) \rangle_{\text{CFT}}. \quad (3.24)$$

Similar to the previous subsection, the four-point twist correlator receives dominant contribution in the large- c limit from the composite twist operator $\mathcal{T}_{n_0}^2$ for which the block is given in eq. (3.6). The cross-ratio x for the four-point twist correlator in eq. (3.24) in this phase is given by

$$x = \frac{(x_3 - x_4)(x_2 + x_4)}{(x_3 + x_4)(x_2 - x_4)}. \quad (3.25)$$

We may now compute the OEE for this phase as follows

$$S_o(A_1 : A_2) = \frac{c}{6} \left[\log \left(\frac{2x_1}{\epsilon} \right) + 2 \log \left(\frac{x_2 - x_3}{\epsilon} \right) + \log \left(\frac{2x_4}{\epsilon} \right) \right] \\ + \frac{c}{6} \log \left[\frac{x_4^2 - x_2 x_3 + \sqrt{(x_4^2 - x_3^2)(x_4^2 - x_2^2)}}{x_4(x_3 - x_2)} \right] + 2S_{\text{bdy}}. \quad (3.26)$$

Similar to the previous case, the entanglement entropy for this phase is same as given in eq. (3.8). Consequently the difference between the OEE and the EE may be obtained as

$$S_o(A_1 : A_2) - S(A_1 \cup A_2) = \frac{c}{6} \log \left[\frac{x_4^2 - x_2 x_3 + \sqrt{(x_4^2 - x_3^2)(x_4^2 - x_2^2)}}{x_4(x_3 - x_2)} \right]. \quad (3.27)$$

Note that the above result matches with the corresponding EWCS obtained in [33, 37, 38] and is consistent with the holographic duality for the OEE in eq. (2.4).

Moving mirror

In order to obtain the OEE for subsystems in moving mirror setup, we may now generalize the OEE obtained for this phase in eq. (3.26) to complex coordinates for subsystems in the RHP at $\tilde{z}_i = (\tilde{t}_i, \tilde{x}_i)$ to obtain an expression same as eq. (3.19) with the modified cross-ratio $\tilde{\eta}$ as

$$\tilde{\eta} = \frac{(\tilde{z}_3 - \tilde{z}_4)(\tilde{z}_2 - \tilde{z}_4^*)}{(\tilde{z}_3 - \tilde{z}_4^*)(\tilde{z}_4 - \tilde{z}_2)}. \quad (3.28)$$

Now, utilizing the inverse of the static map in eq. (2.10), we may obtain the OEE in the moving mirror setup for bipartite state of two disjoint subsystems $A_1 \equiv [(t, x_1), (t, x_2)]$ and $A_2 \equiv [(t, x_3), (t, x_4)]$ as follows given in eq. (3.21) where again the cross-ratio η is modified to

$$\eta = \frac{(p(t-x_3) - p(t-x_4))(p(t-x_2) - t - x_4)}{(p(t-x_3) - t - x_4)(p(t-x_4) - p(t-x_2))}, \quad (3.29)$$

where $p(u)$ represents the mirror profile. The OEE for this configuration modulo the entanglement entropy contribution may be given by

$$S_O(A_1 : A_2) - S(A_1 \cup A_2) = \frac{c}{6} \log \left[\frac{1 + \sqrt{\eta}}{1 - \sqrt{\eta}} \right]. \quad (3.30)$$

We now plot the variation of the difference between the OEE and the EE in fig. 3. In fig. 3a, we plot the difference between the OEE and the EE for escaping mirror in a BCFT₂ described by the mirror profile in eq. (2.13) which mimics an eternal black hole. As expected, the difference starts from a non-zero value at $t = 0$ and starts rising. However after some time it transitions to a different phase, where it ultimately saturates to a constant value. Moreover, fig. 3b depicts the kink mirror setup with the mirror profile given by eq. (2.14) which simulates a evaporating black hole. The difference between the OEE and the EE start from a constant value but after some time transitions to a phase with declining difference, ultimately saturating to a vanishing value.

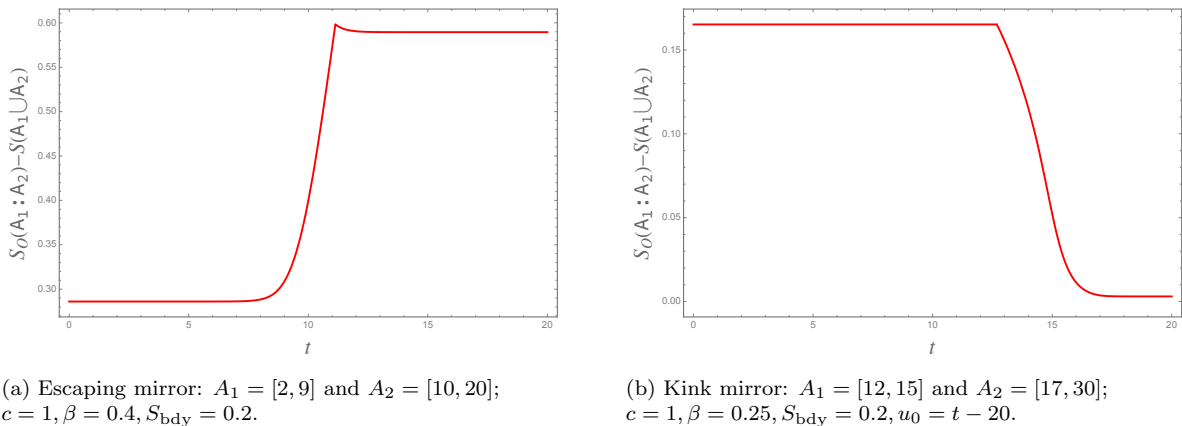


Figure 3: Variation of the difference between the OEE and the EE with time of two disjoint intervals for the escaping and the kink mirrors in BCFT₂.

3.2 OEE for two adjacent subsystems

In this subsection, we obtain the OEE for the mixed state of two adjacent subsystems $A_1 \equiv [x_1, x_2]$ and $A_2 \equiv [x_2, x_3]$ on the half-plane $x \geq 0$ as depicted in fig. 4. This configuration may be obtained by considering the limit $x_2 \rightarrow x_3$ in eq. (3.1) which results in the following three-point twist correlator

$$\text{Tr} \left(\rho_{A_1 A_2}^{T_{A_2}} \right)^{n_0} = \langle \mathcal{T}_{n_0}(x_1) \bar{\mathcal{T}}_{n_0}^2(x_2) \mathcal{T}_{n_0}(x_3) \rangle_{\text{BCFT}}. \quad (3.31)$$

where the conformal dimensions $h_{\mathcal{T}_{n_0}} = \bar{h}_{\bar{\mathcal{T}}_{n_0}} = \bar{h}_{\mathcal{T}_{n_0}^2}$ of \mathcal{T}_{n_0} , $\bar{\mathcal{T}}_{n_0}$ and $\mathcal{T}_{n_0}^2$ are as in eq. (3.2). Using Cardy's doubling trick, we may again express the above three-point twist correlator as a six-point function in the chiral CFT as follows

$$\langle \mathcal{T}_{n_0}(x_1) \bar{\mathcal{T}}_{n_0}^2(x_2) \mathcal{T}_{n_0}(x_3) \rangle_{\text{BCFT}} = \langle \mathcal{T}_{n_0}(x_1) \bar{\mathcal{T}}_{n_0}^2(x_2) \mathcal{T}_{n_0}(x_3) \bar{\mathcal{T}}_{n_0}(-x_1) \mathcal{T}_{n_0}^2(-x_2) \bar{\mathcal{T}}_{n_0}(-x_3) \rangle_{\text{CFT}}. \quad (3.32)$$

The explicit determination of the above six-point twist correlator in the chiral CFT is extremely challenging as it requires the knowledge of the full operator content of the theory. However, it may be evaluated in the large central charge limit for certain cases depending on the location of the subsystems A_1 and A_2 for which the correlation function in eq. (3.32) factorizes. In particular, we observe two different non-trivial phases which are discussed below.

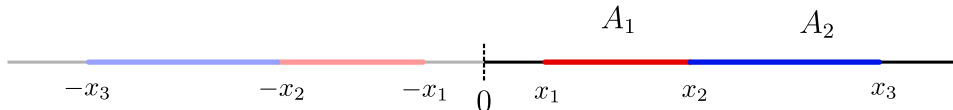


Figure 4: Two adjacent subsystems A_1 and A_2 in BCFT_2 described on half line $x \geq 0$. The darker region on the right ($x > 0$) represents the BCFT_2 and the lighter region on the left ($x < 0$) represent the copy obtained after utilizing the doubling trick.

3.2.1 Phase-I

In this phase, we consider both the subsystems are close to the boundary $x = 0$ and thus the six-point twist correlator in eq. (3.32) factorizes in three two-point correlators as follows

$$\begin{aligned} & \langle \mathcal{T}_{n_0}(x_1) \bar{\mathcal{T}}_{n_0}^2(x_2) \mathcal{T}_{n_0}(x_3) \bar{\mathcal{T}}_{n_0}(-x_1) \mathcal{T}_{n_0}^2(-x_2) \bar{\mathcal{T}}_{n_0}(-x_3) \rangle_{\text{CFT}} \\ & \sim \langle \mathcal{T}_{n_0}(x_1) \bar{\mathcal{T}}_{n_0}(-x_1) \rangle_{\text{CFT}} \langle \bar{\mathcal{T}}_{n_0}^2(x_2) \mathcal{T}_{n_0}^2(-x_2) \rangle_{\text{CFT}} \langle \mathcal{T}_{n_0}(x_3) \bar{\mathcal{T}}_{n_0}(-x_3) \rangle_{\text{CFT}}. \end{aligned} \quad (3.33)$$

By using the standard form of two-point twist correlators in CFT_2 s in the above expression, the OEE for this case may now be obtained through eqs. (2.2) and (2.3) as follows

$$S_o(A_1 : A_2) = \frac{c}{6} \left[\log \left(\frac{2x_1}{\epsilon} \right) + \log \left(\frac{2x_2}{\epsilon} \right) + \log \left(\frac{2x_3}{\epsilon} \right) \right] + 3S_{\text{bdy}}. \quad (3.34)$$

We can read off the entropy contribution for $A_1 \cup A_2$ in the above as follows

$$S(A_1 \cup A_2) = \frac{c}{6} \left[\log \left(\frac{2x_1}{\epsilon} \right) + \log \left(\frac{2x_3}{\epsilon} \right) \right] + 2S_{\text{bdy}}. \quad (3.35)$$

Subtracting this entropy contribution from the OEE in eq. (3.34), we obtain

$$S_o(A_1 : A_2) - S(A_1 \cup A_2) = \frac{c}{6} \log \left(\frac{2x_2}{\epsilon} \right) + S_{\text{bdy}}. \quad (3.36)$$

which matches exactly with the corresponding bulk EWCS computed in [33, 37, 38].

Moving mirror

We will now generalize the above for complex coordinates where the subsystems are now located in the RHP at $\tilde{z}_i = (\tilde{t}_i, \tilde{x}_i)$. Following the above computation, the OEE for this configuration may be computed easily to be

$$S_o(A_1 : A_2) = \frac{c}{6} \left[\log \left(\frac{\tilde{z}_1 - \tilde{z}_1^*}{\epsilon} \right) + \log \left(\frac{\tilde{z}_2 - \tilde{z}_2^*}{\epsilon} \right) + \log \left(\frac{\tilde{z}_3 - \tilde{z}_3^*}{\epsilon} \right) \right] + 3S_{\text{bdy}}. \quad (3.37)$$

where as earlier \tilde{z}_i^* is the complex conjugate of \tilde{z}_i . Finally, inverting the static mirror map in eq. (2.10), the OEE for subsystems $A_1 \equiv [(t, x_1), (t, x_2)]$ and $A_2 \equiv [(t, x_2), (t, x_3)]$ may be obtained to be

$$S_o(A_1 : A_2) = \frac{c}{6} \left[\log \left(\frac{p(t-x_1) - t - x_1}{\epsilon \sqrt{p'(t-x_1)}} \right) + \log \left(\frac{p(t-x_2) - t - x_2}{\epsilon \sqrt{p'(t-x_2)}} \right) + \log \left(\frac{p(t-x_3) - t - x_3}{\epsilon \sqrt{p'(t-x_3)}} \right) \right] + 3S_{\text{bdy}}, \quad (3.38)$$

where $p(u)$ represents the specific mirror profile and the square roots in the denominator arise from the transformation of the correlators to the moving mirror setup. The entropy contribution for $A_1 \cup A_2$ may be obtained in the present scenario to be

$$S_o(A_1 : A_2) = \frac{c}{6} \left[\log \left(\frac{p(t-x_1) - t - x_1}{\epsilon \sqrt{p'(t-x_1)}} \right) + \log \left(\frac{p(t-x_3) - t - x_3}{\epsilon \sqrt{p'(t-x_3)}} \right) \right] + 2S_{\text{bdy}}, \quad (3.39)$$

Subtracting this entropy contribution from the OEE obtained in eq. (3.38), we obtain

$$S_o(A_1 : A_2) - S(A_1 \cup A_2) = \frac{c}{6} \log \left(\frac{p(t-x_2) - t - x_2}{\epsilon \sqrt{p'(t-x_2)}} \right) + S_{\text{bdy}}. \quad (3.40)$$

which again matches with the corresponding bulk EWCS computed [33].

3.2.2 Phase-II

In this phase, we consider that the subsystem A_1 is close to the boundary and is large in comparison to subsystem A_2 such that the three-point BCFT correlator in eq. (3.31) factorizes as follows

$$\langle \mathcal{T}_{n_0}(x_1) \bar{\mathcal{T}}_{n_0}^2(x_2) \mathcal{T}_{n_0}(x_3) \rangle_{\text{BCFT}} \sim \langle \mathcal{T}_{n_0}(x_1) \rangle_{\text{BCFT}} \langle \bar{\mathcal{T}}_{n_0}^2(x_2) \mathcal{T}_{n_0}(x_3) \rangle_{\text{BCFT}}. \quad (3.41)$$

The above two-point correlator on the half plane may be expressed in terms of a three-point twist field correlator in a CFT as follows [33, 40]

$$\langle \bar{\mathcal{T}}_{n_0}^2(x_2) \mathcal{T}_{n_0}(x_3) \rangle_{\text{BCFT}} \sim \langle \mathcal{T}_{n_0}(-x_3) \bar{\mathcal{T}}_{n_0}^2(x_2) \bar{\mathcal{T}}_{n_0}(x_3) \rangle_{\text{CFT}}. \quad (3.42)$$

The corresponding OEE for this configuration may now be computed by using eqs. (2.2) and (2.3) as follows

$$S_o(A_1 : A_2) = \frac{c}{6} \left[\log \left(\frac{x_3 - x_2}{\epsilon} \right) + \log \left(\frac{x_2 + x_3}{\epsilon} \right) + \log \left(\frac{2x_3}{\epsilon} \right) + \log \left(\frac{2x_1}{\epsilon} \right) \right] + 2S_{\text{bdy}}. \quad (3.43)$$

The entanglement entropy for this phase remains unchanged and is given by eq. (3.35). The OEE excluding the contribution from the entanglement entropy may then be obtained as

$$S_o(A_1 : A_2) - S(A_1 \cup A_2) = \frac{c}{6} \log \left(\frac{x_3^2 - x_2^2}{\epsilon(2x_3)} \right), \quad (3.44)$$

which matches the corresponding EWCS [33, 37, 38] apart from an additive constant. An explicit analysis of the OPE coefficient of the corresponding three-point twist correlator in eq. (3.42) in lines of [7] may lead to the recovery of this constant.

Moving mirror

We now proceed to generalize the above computation for complex coordinates in the RHP with coordinates $\tilde{z} = (\tilde{t}, \tilde{x})$. The OEE for subsystems in this RHP may be obtained similarly as

$$S_o(A_1 : A_2) = \frac{c}{6} \left[\log \left(\frac{z_3 - z_2}{\epsilon} \right) + \log \left(\frac{z_3 - z_2^*}{\epsilon} \right) + \log \left(\frac{z_3 - z_3^*}{\epsilon} \right) + \log \left(\frac{z_1 - z_1^*}{\epsilon} \right) \right] + 2S_{\text{bdy}}. \quad (3.45)$$

where the endpoints of the subsystems are $\tilde{z}_i = (\tilde{t}_i, \tilde{x}_i)$ and \tilde{z}_i^* are their complex conjugates. Again, inverting the static mirror map in eq. (2.10), we may obtain the OEE for subsystems $A_1 \equiv [(t, x_1), (t, x_2)]$ and $A_2 \equiv [(t, x_2), (t, x_3)]$ in the moving mirror setup to be

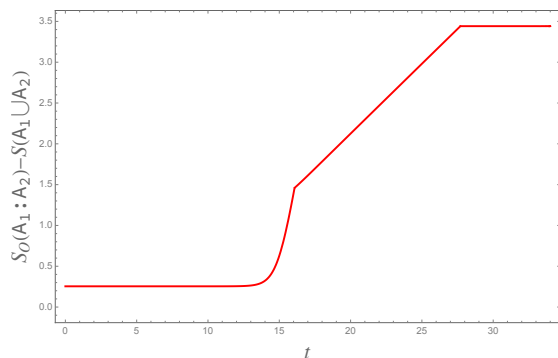
$$S_o(A_1 : A_2) = \frac{c}{6} \left[\log \left(\frac{p(t-x_3) - p(t-x_2)}{\epsilon \sqrt{p'(t-x_2)p'(t-x_3)}} \right) + \log \left(\frac{t+x_3 - p(t-x_2)}{\epsilon \sqrt{p'(t-x_2)}} \right) \right. \\ \left. + \log \left(\frac{p(t-x_3) - t-x_3}{\epsilon \sqrt{p'(t-x_1)}} \right) + \log \left(\frac{p(t-x_1) - t-x_1}{\epsilon \sqrt{p'(t-x_1)}} \right) \right] + 2S_{\text{bdy}}, \quad (3.46)$$

where, like earlier, the function $p(u)$ represents the specific mirror profile and the square root in the denominator is due to the transformation of the corresponding correlation function to the moving mirror setup. The entanglement entropy for this case, as stated earlier, remains same as the previous case in eq. (3.39). Subtracting this entropy contribution, we may obtain the following

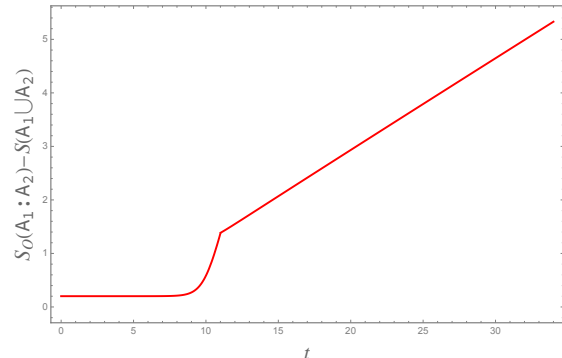
$$S_o(A_1 : A_2) - S(A_1 \cup A_2) = \frac{c}{6} \left[\log \left(\frac{p(t-x_2) - p(t-x_1)}{\epsilon \sqrt{p'(t-x_2)p'(t-x_1)}} \right) + \log \left(\frac{p(t-x_2) - t-x_1}{\epsilon \sqrt{p'(t-x_2)}} \right) \right. \\ \left. - \log \left(\frac{p(t-x_1) - t-x_1}{\epsilon \sqrt{p'(t-x_1)}} \right) \right], \quad (3.47)$$

which matches the corresponding result for the EWCS in [33] up to an additive constant.

We now plot the variation of the difference between the OEE and the EE in fig. 5. Fig. 5a depicts the difference between the OEE and the EE for two adjacent intervals for escaping mirror in a BCFT₂ with the mirror profile eq. (2.13). For the given values of the parameters in this case, the OEE transits from **phase-II** to **phase-I** at $t \approx 16$. However it returns back to **phase-II** at $t \approx 28$ and saturates at a constant value beyond that. Furthermore, fig. 5b depicts the kink mirror setup with the mirror profile given by eq. (2.14) which simulates an evaporating black hole. Again in this case, we observe a transition from **phase-II** to **phase-I** at $t \approx 11$. But unlike the escaping mirror case, the OEE stays in **phase-I** indefinitely beyond this time.



(a) Escaping mirror: $A_1 = [2, 15]$ and $A_2 = [15, 18]$; $c = 1, \beta = 0.5, S_{\text{bdy}} = 0.2, \epsilon = 0.05$.



(b) Kink mirror: $A_1 = [2, 10]$ and $A_2 = [10, 15]$; $c = 1, \beta = 0.5, S_{\text{bdy}} = 0.2, \epsilon = 0.05, u_0 = t - 20$.

Figure 5: Variation of the difference between the OEE and the EE with time of two adjacent intervals for the escaping and the kink mirrors in BCFT₂.

4 Summary and conclusions

In this article, we have investigated the mixed state entanglement structure of bipartite subsystems in BCFT_2 s through the OEE by utilizing a suitable replica technique. We have compared our results with earlier literature to verify the validity of its holographic duality with the EWCS in the $\text{AdS}_3/\text{BCFT}_2$ framework. Furthermore we have extended our computations to the holographic moving mirror setup which simulates the Hawking radiation from a black hole.

For the configuration of two disjoint intervals, we have utilized the doubling trick to describe the OEE for this configuration through an eight-point twist correlator in the chiral CFT. This eight-point correlator factorized in various ways in the large central charge limit, leading to three unique non-trivial phases for the OEE depending upon the location and size of the subsystems. We obtain the OEE for all these phases and found consistent matching of the difference between the OEE and the EE with the bulk EWCS, which provides a significant consistency check for our computations. We further generalize these computations to obtain the OEE for moving mirror setup. Moreover, we plot the variation of the difference between the OEE and the EE with time to observe the transition between the various phases. In particular we plot this variation for two specific mirror profiles mimicking an eternal black hole and an evaporating black hole.

We also consider the bipartite mixed state described by two adjacent subsystems in BCFT_2 s. For this case, the OEE is characterized by a three-point BCFT twist field correlator, or a six-point chiral CFT correlator. Again, in the large- c limit, this correlator may be factorized in various ways depending upon the subsystem size and location. In particular we observe two distinct non-trivial phases for which the OEE has been computed. The consistency of our computations have been verified by comparing the difference of the OEE and the EE with the bulk EWCS obtained earlier. We again extend the OEE to the case of moving mirrors. We finally plot the variation of the difference between the OEE and the EE for this configuration in moving mirror setup to observe transition between the two phases.

In the present setup, the variations of the OEE with time is indicative of a rich phase structure of the mixed state entanglement in the Hawking radiation simulated by the moving mirrors which requires further investigations in other models of black hole evaporation like [41–49]. A deeper understanding of this phase structure could be obtained by studying the methods of information recovery for mixed states from the black hole interior which seem to involve non-isometric encoding of the interior degrees of freedom [50, 51]. It would also be interesting to explicitly investigate the OEE for mixed states in island formalism by constructing an island formula for the OEE. We leave these exciting issues for future investigations.

Acknowledgement

The authors would like to thank Debarshi Basu for several helpful discussions. The work of GS is partially supported by the Dr Jagmohan Garg Chair Professor position at the Indian Institute of Technology, Kanpur.

References

- [1] P. Calabrese and J. L. Cardy, “Entanglement entropy and quantum field theory,” [*J. Stat. Mech.* **0406** \(2004\) P06002](#), [arXiv:hep-th/0405152](#).
- [2] P. Calabrese and J. Cardy, “Entanglement entropy and conformal field theory,” [*J. Phys. A* **42** \(2009\) 504005](#), [arXiv:0905.4013 \[cond-mat.stat-mech\]](#).
- [3] G. Vidal and R. F. Werner, “Computable measure of entanglement,” [*Phys. Rev. A* **65** \(2002\) 032314](#), [arXiv:quant-ph/0102117](#).

- [4] M. B. Plenio, “Logarithmic Negativity: A Full Entanglement Monotone That is not Convex,” [*Phys. Rev. Lett.* **95** \(2005\) 090503](#), [arXiv:quant-ph/0505071](#).
- [5] T. Takayanagi and K. Umemoto, “Entanglement of purification through holographic duality,” [*Nature Phys.* **14** no. 6, \(2018\) 573–577](#), [arXiv:1708.09393 \[hep-th\]](#).
- [6] P. Nguyen, T. Devakul, M. G. Halbasch, M. P. Zaletel, and B. Swingle, “Entanglement of purification: from spin chains to holography,” [*JHEP* **01** \(2018\) 098](#), [arXiv:1709.07424 \[hep-th\]](#).
- [7] S. Dutta and T. Faulkner, “A canonical purification for the entanglement wedge cross-section,” [*JHEP* **03** \(2021\) 178](#), [arXiv:1905.00577 \[hep-th\]](#).
- [8] Q. Wen, “Balanced Partial Entanglement and the Entanglement Wedge Cross Section,” [*JHEP* **04** \(2021\) 301](#), [arXiv:2103.00415 \[hep-th\]](#).
- [9] K. Tamaoka, “Entanglement Wedge Cross Section from the Dual Density Matrix,” [*Phys. Rev. Lett.* **122** no. 14, \(2019\) 141601](#), [arXiv:1809.09109 \[hep-th\]](#).
- [10] J. M. Maldacena, “The Large N limit of superconformal field theories and supergravity,” [*Adv. Theor. Math. Phys.* **2** \(1998\) 231–252](#), [arXiv:hep-th/9711200](#).
- [11] E. Witten, “Anti-de Sitter space and holography,” [*Adv. Theor. Math. Phys.* **2** \(1998\) 253–291](#), [arXiv:hep-th/9802150](#).
- [12] Y. Kusuki and K. Tamaoka, “Entanglement Wedge Cross Section from CFT: Dynamics of Local Operator Quench,” [*JHEP* **02** \(2020\) 017](#), [arXiv:1909.06790 \[hep-th\]](#).
- [13] A. Mollabashi and K. Tamaoka, “A Field Theory Study of Entanglement Wedge Cross Section: Odd Entropy,” [*JHEP* **08** \(2020\) 078](#), [arXiv:2004.04163 \[hep-th\]](#).
- [14] X. Dong, X.-L. Qi, and M. Walter, “Holographic entanglement negativity and replica symmetry breaking,” [*JHEP* **06** \(2021\) 024](#), [arXiv:2101.11029 \[hep-th\]](#).
- [15] M. Ghasemi, A. Naseh, and R. Pirmoradian, “Odd entanglement entropy and logarithmic negativity for thermofield double states,” [*JHEP* **10** \(2021\) 128](#), [arXiv:2106.15451 \[hep-th\]](#).
- [16] J. K. Basak, H. Chourasiya, V. Raj, and G. Sengupta, “Odd entanglement entropy in Galilean conformal field theories and flat holography,” [*Eur. Phys. J. C* **82** no. 11, \(2022\) 1050](#), [arXiv:2203.03902 \[hep-th\]](#).
- [17] D. Basu, S. Biswas, A. Dey, B. Paul, and G. Sengupta, “Odd Entanglement Entropy in $T\bar{T}$ deformed CFT_{2S} and Holography,” [arXiv:2307.04832 \[hep-th\]](#).
- [18] J. L. Cardy, “Boundary conformal field theory,” [arXiv:hep-th/0411189](#).
- [19] J. Sully, M. Van Raamsdonk, and D. Wakeham, “BCFT entanglement entropy at large central charge and the black hole interior,” [*JHEP* **03** \(2021\) 167](#), [arXiv:2004.13088 \[hep-th\]](#).
- [20] T. Takayanagi, “Holographic Dual of BCFT,” [*Phys. Rev. Lett.* **107** \(2011\) 101602](#), [arXiv:1105.5165 \[hep-th\]](#).
- [21] M. Fujita, T. Takayanagi, and E. Tonni, “Aspects of AdS/BCFT,” [*JHEP* **11** \(2011\) 043](#), [arXiv:1108.5152 \[hep-th\]](#).

- [22] I. Akal, Y. Kusuki, N. Shiba, T. Takayanagi, and Z. Wei, “Entanglement Entropy in a Holographic Moving Mirror and the Page Curve,” [*Phys. Rev. Lett.* **126** no. 6, \(2021\) 061604](#), [arXiv:2011.12005 \[hep-th\]](#).
- [23] I. Akal, Y. Kusuki, N. Shiba, T. Takayanagi, and Z. Wei, “Holographic moving mirrors,” [*Class. Quant. Grav.* **38** no. 22, \(2021\) 224001](#), [arXiv:2106.11179 \[hep-th\]](#).
- [24] S. W. Hawking, “Particle Creation by Black Holes,” [*Commun. Math. Phys.* **43** \(1975\) 199–220](#). [Erratum: *Commun.Math.Phys.* 46, 206 (1976)].
- [25] P. C. W. Davies and S. A. Fulling, “Radiation from a moving mirror in two-dimensional space-time conformal anomaly,” [*Proc. Roy. Soc. Lond. A* **348** \(1976\) 393–414](#).
- [26] N. D. Birrell and P. C. W. Davies, [*Quantum Fields in Curved Space*](#). Cambridge Monographs on Mathematical Physics. Cambridge Univ. Press, Cambridge, UK, 2, 1984.
- [27] M. R. R. Good, E. V. Linder, and F. Wilczek, “Moving mirror model for quasithermal radiation fields,” [*Phys. Rev. D* **101** no. 2, \(2020\) 025012](#), [arXiv:1909.01129 \[gr-qc\]](#).
- [28] M. R. R. Good, “Extremal Hawking radiation,” [*Phys. Rev. D* **101** no. 10, \(2020\) 104050](#), [arXiv:2003.07016 \[gr-qc\]](#).
- [29] Y. Sato, “Complexity in a moving mirror model,” [*Phys. Rev. D* **105** no. 8, \(2022\) 086016](#), [arXiv:2108.04637 \[hep-th\]](#).
- [30] D. S. Ageev, “Shaping contours of entanglement islands in BCFT,” [*JHEP* **03** \(2022\) 033](#), [arXiv:2107.09083 \[hep-th\]](#).
- [31] I. A. Reyes, “Moving Mirrors, Page Curves, and Bulk Entropies in AdS₂,” [*Phys. Rev. Lett.* **127** no. 5, \(2021\) 051602](#), [arXiv:2103.01230 \[hep-th\]](#).
- [32] K. Kawabata, T. Nishioka, Y. Okuyama, and K. Watanabe, “Probing Hawking radiation through capacity of entanglement,” [*JHEP* **05** \(2021\) 062](#), [arXiv:2102.02425 \[hep-th\]](#).
- [33] J. Basak Kumar, D. Basu, V. Malvimat, H. Parihar, and G. Sengupta, “Reflected entropy and entanglement negativity for holographic moving mirrors,” [*JHEP* **09** \(2022\) 089](#), [arXiv:2204.06015 \[hep-th\]](#).
- [34] I. Akal, T. Kawamoto, S.-M. Ruan, T. Takayanagi, and Z. Wei, “Zoo of holographic moving mirrors,” [*JHEP* **08** \(2022\) 296](#), [arXiv:2205.02663 \[hep-th\]](#).
- [35] M. R. R. Good, A. Lapponi, O. Luongo, and S. Mancini, “Modeling black hole evaporative mass evolution via radiation from moving mirrors,” [*Phys. Rev. D* **107** no. 10, \(2023\) 104004](#), [arXiv:2210.09744 \[gr-qc\]](#).
- [36] P. Kumar, I. A. Reyes, and J. Wintergerst, “Relativistic dynamics of moving mirrors in CFT₂: quantum backreaction and black holes,” [arXiv:2310.03483 \[hep-th\]](#).
- [37] Y. Lu and J. Lin, “The Markov gap in the presence of islands,” [*JHEP* **03** \(2023\) 043](#), [arXiv:2211.06886 \[hep-th\]](#).
- [38] D. Basu, J. Lin, Y. Lu, and Q. Wen, “Ownerless island and partial entanglement entropy in island phases,” [arXiv:2305.04259 \[hep-th\]](#).
- [39] P. Calabrese, J. Cardy, and E. Tonni, “Entanglement negativity in quantum field theory,” [*Phys. Rev. Lett.* **109** \(2012\) 130502](#), [arXiv:1206.3092 \[cond-mat.stat-mech\]](#).

- [40] T. Li, M.-K. Yuan, and Y. Zhou, “Defect extremal surface for reflected entropy,” [JHEP](#) **01** (2022) 018, [arXiv:2108.08544 \[hep-th\]](#).
- [41] V. Balasubramanian, A. Kar, O. Parrikar, G. Sárosi, and T. Ugajin, “Geometric secret sharing in a model of Hawking radiation,” [JHEP](#) **01** (2021) 177, [arXiv:2003.05448 \[hep-th\]](#).
- [42] V. Balasubramanian, A. Kar, and T. Ugajin, “Entanglement between two disjoint universes,” [JHEP](#) **02** (2021) 136, [arXiv:2008.05274 \[hep-th\]](#).
- [43] E. Verheijden and E. Verlinde, “From the BTZ black hole to JT gravity: geometrizing the island,” [JHEP](#) **11** (2021) 092, [arXiv:2102.00922 \[hep-th\]](#).
- [44] C. Akers, N. Engelhardt, and D. Harlow, “Simple holographic models of black hole evaporation,” [JHEP](#) **08** (2020) 032, [arXiv:1910.00972 \[hep-th\]](#).
- [45] G. Penington, S. H. Shenker, D. Stanford, and Z. Yang, “Replica wormholes and the black hole interior,” [JHEP](#) **03** (2022) 205, [arXiv:1911.11977 \[hep-th\]](#).
- [46] V. Balasubramanian, B. Craps, M. Khramtsov, and E. Shaghoulian, “Submerging islands through thermalization,” [JHEP](#) **10** (2021) 048, [arXiv:2107.14746 \[hep-th\]](#).
- [47] M. Afrasiar, D. Basu, A. Chandra, V. Raj, and G. Sengupta, “Islands and dynamics at the interface,” [arXiv:2306.12476 \[hep-th\]](#).
- [48] D. Basu, Q. Wen, and S. Zhou, “Entanglement Islands from Hilbert Space Reduction,” [arXiv:2211.17004 \[hep-th\]](#).
- [49] D. Basu, H. Parihar, V. Raj, and G. Sengupta, “Defect extremal surfaces for entanglement negativity,” [arXiv:2205.07905 \[hep-th\]](#).
- [50] V. Balasubramanian, A. Kar, C. Li, and O. Parrikar, “Quantum error correction in the black hole interior,” [JHEP](#) **07** (2023) 189, [arXiv:2203.01961 \[hep-th\]](#).
- [51] C. Akers, N. Engelhardt, D. Harlow, G. Penington, and S. Vardhan, “The black hole interior from non-isometric codes and complexity,” [arXiv:2207.06536 \[hep-th\]](#).